
Article:
Liu, S. orcid.org/0009-0008-5660-1063, Dong, J., Ma, Z. et al. (6 more authors) (2024) The evolution of indium precipitation in gallium focused ion beam prepared samples of InGaAs/InAlAs quantum wells under electron beam irradiation. Journal of Microscopy, 293 (3). pp. 169-176. ISSN 0022-2720

https://doi.org/10.1111/jmi.13251

The evolution of indium precipitation in gallium focused ion beam prepared samples of InGaAs/InAlAs quantum wells under electron beam irradiation

Shuo Liu[1*], Jiawei Dong[1*], Zhenyu Ma[1], Wenyu Hu[2], Yong Deng[1,2], Yuechun Shi[3], Xiaoyi Wang[1], Yang Qiu[2#] and Thomas Walther[4]

[1] Southwest Minzu University, State Ethnic Affairs Commission, Chengdu 610041, China

[2] Pico center, SUSTech Core Research Facilities, Southern University of Science and Technology, Shenzhen 518055, China

[3] Yongjiang Laboratory, Ningbo 315000, China

[4] Dept. Electronic & Electrical Eng., University of Sheffield, Sheffield S1 3JD, UK

Correspondence

Pico center, SUSTech Core Research, Facilities, Southern University of Science and Technology, Shenzhen 518055, China; Email: qiuy@sustech.edu.cn

Abstract

Gallium ion (Ga^+) beam damage induced indium (In) precipitation in indium gallium arsenide (InGaAs) / indium aluminium arsenide (InAlAs) multiple quantum wells and its corresponding evolution under electron beam irradiation was investigated by valence electron energy loss spectroscopy（VEELS）and high-angle annular dark field imaging (HAADF) in scanning transmission electron microscopy (STEM). Compared with argon ion milling for sample preparation, the heavier projectiles of Ga^+ ions pose a risk to trigger In formation in the form of tiny metallic In clusters. These are shown to be sensitive to electron irradiation and can increase in number and size under the electron beam, deteriorating the structure. Our finding reveals the potential risk of formation of In clusters during focused ion beam (FIB) preparation of InGaAs/InAlAs quantum well samples and their subsequent growth under STEM-HAADF imaging, where initially invisible In clusters of a few atoms can move and swell during electron beam exposure.

Keywords: STEM, HAADF, In precipitation, QCL, InGaAs/InAlAs

1 INTRODUCTION

To achieve long wavelength photon emission, the fabrication of high indium content III-V ternary alloys is a promising approach. However, the growth of high In content III-V nitrides quantum wells often suffers from In segregation during growth.[1-4] The formation of In-rich semiconducting clusters or even metallic In clusters is expected to localize the electrons, and the change of the local density of states（DOS）would degrade the optical properties.[5-7] On the practical side, high-angle annular dark-field scanning transmission electron microscopy (HAADF-STEM) provides the possibility of observing In segregation or precipitation at the sub-nanometer scale because HAADF-STEM is very sensitive to changes in average atomic numbers (*Z*-contrast), which allows the observation of In segregation[8] and compositional variations.[9] In InGaAs/InAlAs quantum wells, due to the large atomic number of In, segregation of In atoms increases the local intensity in HAADF images, which allows a direct mapping of In-rich nano-clusters.[10]

In current specimen preparation techniques for transmission electron microscopy（TEM）, gallium (Ga) focused ion beam (FIB) instruments play a significant role, due to the advantages of low volatility,[11] fast milling rates[12-13] and fine probe sizes,[14] and have gradually replaced the more traditional argon (Ar) broad ion beam milling. With FIBs reaching a spatial resolution of ~ 7 nm,[15] they also have a wide application in nano-structure fabrication.[16] The major issue of Ga^+-FIB prepared III-V semiconductor lamellas is ion beam induced Ga^+ implantation. Different from lighter ions such as helium or argon, Ga^+ ions are able to produce cascades of recoil atoms, separating interstitials and vacancies to a large extent, which can produce a problem if short-range recombination of interstitials and vacancies (Frenkel pair recombination) is energetically unfavourable.[17] The combination of FIB fabrication of electron transparent lamellas and TEM imaging plays an important role in nano-device processing and characterization. Therefore, it is vital to understand the Ga^+ ion induced damage in compound semiconductors as well as its evolution under electron beam scanning.

The mechanisms of Ga^+ ion implantation into III-V semiconductors have been established,[18] and it was found that Ga^+ implantation into InGaN may produce metallic In clusters during the Ga^+ ion irradiation, which can be attributed to the lower displacement energy of In than Ga[19]. Besides, the ionization enhanced diffusion may also be significant.[20]

As far as In based ternary nitride alloys are concerned, it was soon recognized that a high-energetic electron beam (≥200 kV)[21] at high dose rate during imaging can also influence the formation and evolution of In-rich clusters.[22-23] Ionization enhanced diffusion[24] may also influence cluster size and shape under electron irradiation. These effects have been mainly observed in InGaN quantum well systems,[25] however, they have not been reported so far for InGaAs/InAlAs based multiple quantum wells.

Therefore, in this work, segregation in indium-rich InGaAs/InAlAs multiple quantum wells and their corresponding response to electron beam irradiation is investigated. By exploiting FIB to prepare a TEM lamella, implanted Ga^+ ions are expected to lead to In segregation and precipitation.[17] Afterwards electron beam irradiation was performed in a scanning transmission electron microscope, where the dynamical change of indium-rich clusters was studied by prolonged HAADF-STEM.[26] We confirmed that conventional Ar^+ ion milling did not lead to any observable indium segregation within the quantum wells. Subsequently, each FIB prepared lamella was subjected to continuous scanning at the same dose to capture further images at different time points, aiming to investigate any size and morphological changes within the quantum wells as a function of electron irradiation time. Continuous scanning was performed in STEM mode for different times. Through lattice imaging, the dynamic influence of electron beam irradiation on the distribution of In within the quantum wells was studied. Significant nanoscale aggregation of In was induced in multiple quantum wells prepared by Ga^+ ions but not in those prepared by Ar^+ ions. These findings emphasize the need for caution when studying FIB prepared In-based III-V quantum well specimens using TEM even in the In(Ga,Al)As system, as the initially formed In-rich clusters are so small they can remain invisible for some time.

2 EXPERIMENTAL PROCEDURES

The epitaxy of InGaAs/InAlAs multiple quantum wells on an InP (001) substrate with a 200 nm InGaAs buffer layer was carried out in a 2800 G4 Aixtron reactor for metal organic vapour deposition (MOCVD). Trimethylaluminium (TMAl), trimethylgallium (TMGa), trimethylindium (TMIn) and AsH_3 were used as precursors. The growth temperature for InGaAs quantum wells was 655°C and that for InAlAs barrier layers was 625°C. This alternating growth process was repeated to obtain a sample for a quantum cascade laser (QCL).

For Ga implantation and lamella production a FEI Helios 600i FIB system was applied. To protect the sample surface during the ion milling, a spin-on-carbon (SOC) layer had been deposited on the wafer pieces. A ~300 nm Pt layer was deposited afterwards to further protect the region of interest. A 30 kV Ga^+ ion beam with a beam current of 0.23-9.3 nA was used for producing the lamella, while a 2kV Ga^+ ion beam with a beam current of ~23 pA was performed to produce the final ~50 nm thick sample. For the Ar^+ ion milled sample, an Allied 69-42000 tripod polisher was used to first mechanically grind and polish the specimen wedge down to ~15 µm (wedge angle was set as 1.5° to avoid the sample crack at the tip), and a Fischione Nanomill 1040 was then used to produce an electron transparent region, where a 2 kV Ar^+ ion beam with a beam current ~150 pA was used. The final surface polishing was conducted at 900 eV with a beam current of ~150 pA. To reveal the evolution of In segregation under electron beam irradiation, a Thermo-Fisher Titan cubed THEMIS G2 equipped with a sperical aberration corrector and a monochromator was applied, capable of achieving a spatial resolution down to 60 pm at 300 kV as well as recording valence electron energy loss spectra (VEELS) with 170 meV energy resolution at 60 kV for the analysis of In segregation of the QCL materials. Energy dispersive X-ray spectroscopy (EDXS) elemental maps were recorded using Super-X silicon drift detectors, where the energy resolution and collection angle were nominally 136 eV and 0.9 srad, respectively.

3 RESULTS AND DISCUSSION

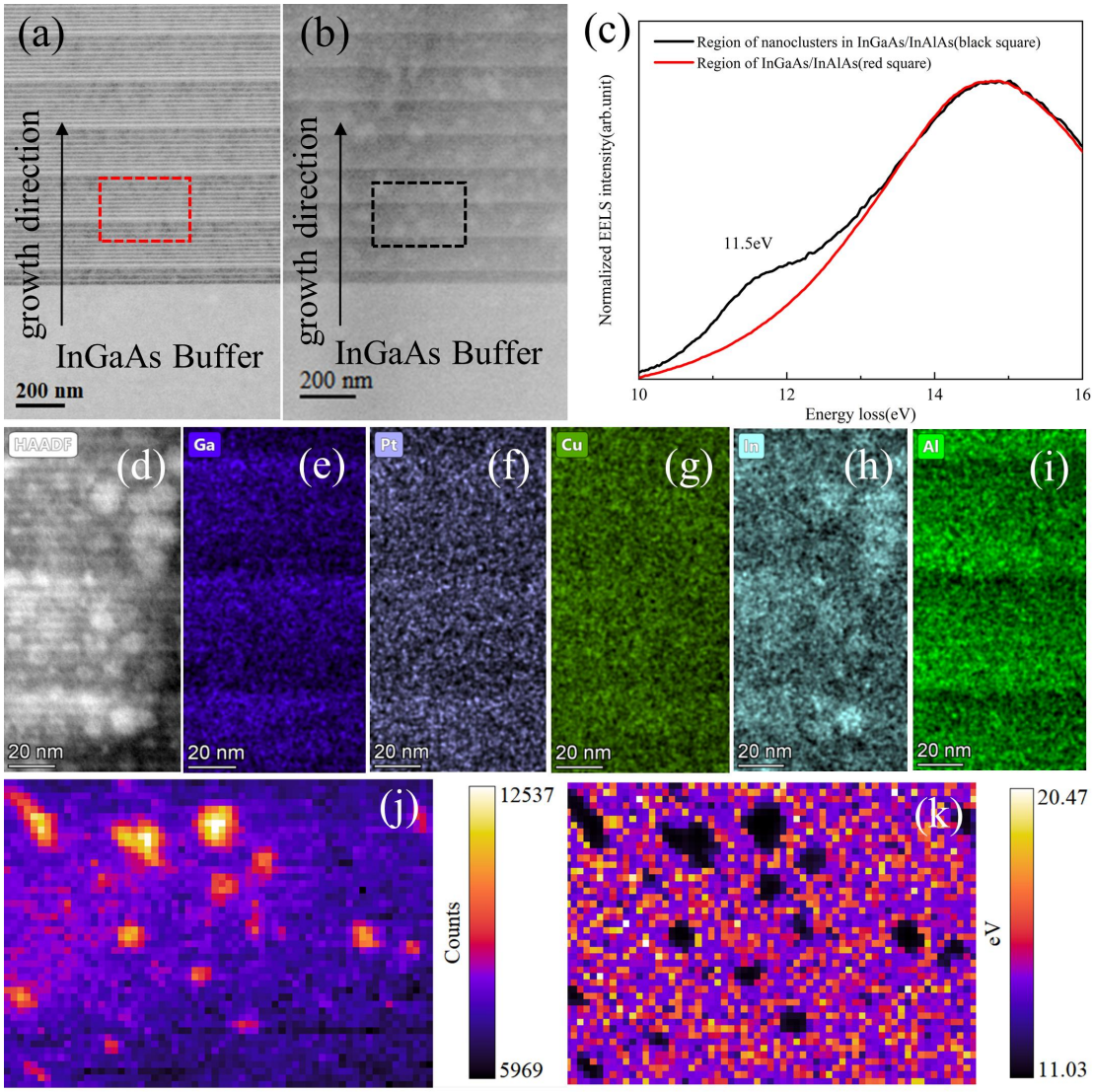

Figure 1: ADF overview images of multiple quantum wells prepared by (a) Ar^+ polishing and (b) Ga^+-FIB; (c) electron energy loss spectroscopy at 60 kV of regions indicated in (a) and (b) where the red line refers to (a) and the black line to (b); HAADF (d) and EDXS mapping (e-i) of sample shown in (b); distribution map of peak plasmon loss energy (j) and indium plasmon peak intensity (k) for energy window of 1 eV centered around 11.5 eV (from 11 eV to 12 eV) of sample shown in (b).

We observe the evolution during electron irradiation of In-rich clusters formed under Ga^+ ion bombardment via HAADF imaging, EDXS and VEELS. As can be

seen in Fig. 1 (b), bright nanoparticles are observed for the FIB prepared TEM sample only while they are absent from the Ar^+ ion milled specimen shown in Fig. 1 (a). According to the elemental X-ray maps in Figs. 1 (e)-(i), the clusters in the Ga^+-FIB produced specimen are In rich while no Cu, Ga or Pt signals can be found in these clusters. To determine the chemical constitution of the nanoclusters, VEEL spectra have been extracted from regions without and with In-rich nanoparticles and are displayed in Fig. 1 (c). Here, a shoulder near ~11.5 eV is observed in the FIB-prepared sample only, which correlates well with the plasmon energy of metallic In while In-rich InGaAs would have produced a plasmon peak nearer 14 eV, as for InAs.[27] By modelling the In plasmon peak as a Lorentzian function, maps of the plasmon peak energy (Fig. 1 (j)) and its corresponding intensity distribution (Fig. 1 (k)) are calculated. The intensive In plasmon resonance at 11.5 eV was only found at the position of the nanoclusters, which indicates In precipitation induced by Ga^+ ion bombardment has led to the formation of metallic indium particles, while no formation of such In clusters was observed after Ar^+ ion thinning.

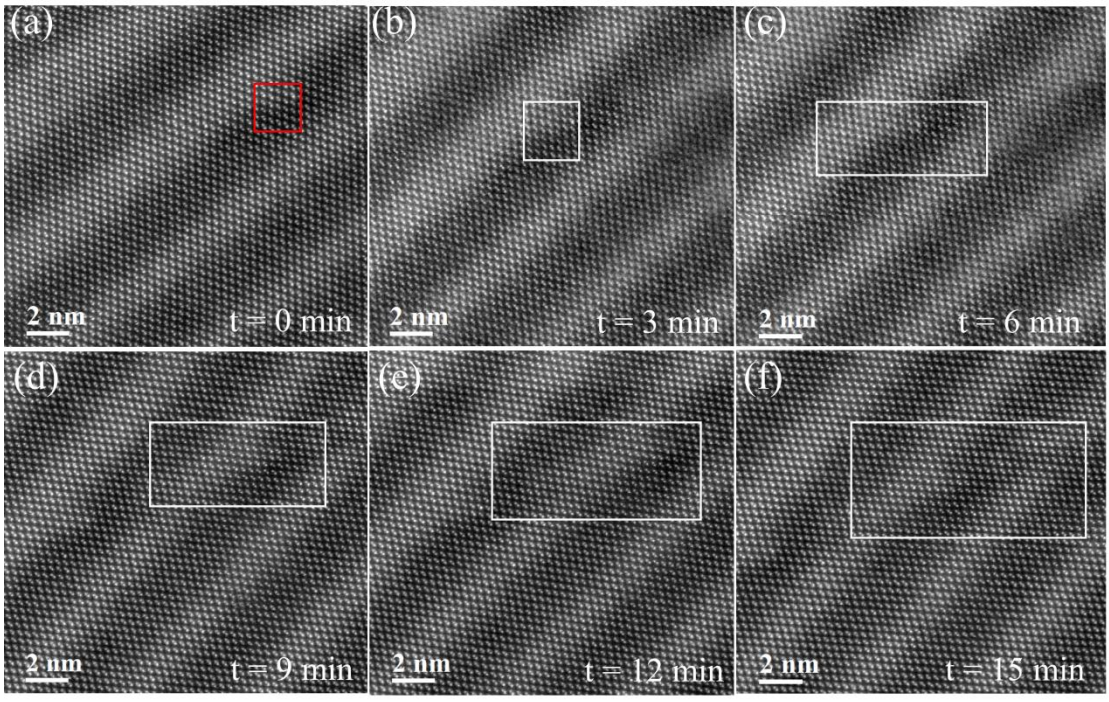

Figure 2: (a-f) Continuous HAADF-STEM imaging at 300 kV of the same region shows In clusters multiplying and expanding. For the HAADF-STEM imaging, we adopted a probe size of ~ 1 Å with a beam current of 47 pA, the dwell time was set as

4 μs with a scan speed of ~2.18×10^5 pixel per second, so the dose can be estimated as 8.92×10^{19} electrons/cm^2 during the image acquisition.

To study the evolution of In segregation under high energy electron irradiation, a 25 mrad convergent, aberration corrected electron beam of approximate probe size of < 1 Å was formed and continuously raster scanned over the sample, so the small In-rich regions can be resolved at atomic scale. The acquired HAADF-STEM lattice images at fixed time intervals are shown in Fig. 2. At the start of electron beam scanning (t = 0 min), a tiny In nano-precipitate (maybe a few In atoms only) with bright contrast was noticed near the bottom of one of the InGaAs interfaces (red square). After 3 minutes exposure to the electron beam, a clear intensity variation has been observed near the quantum well (white square in Fig. 2 (b)), which probably indicates that In segregation has been promoted under the continuous electron exposure. By continuously scanning the sample for 15 minutes (Figs. 2 (c)-(f)), the size of the In-rich region was observed to grow by cation interdiffusion on {111} lattice planes.

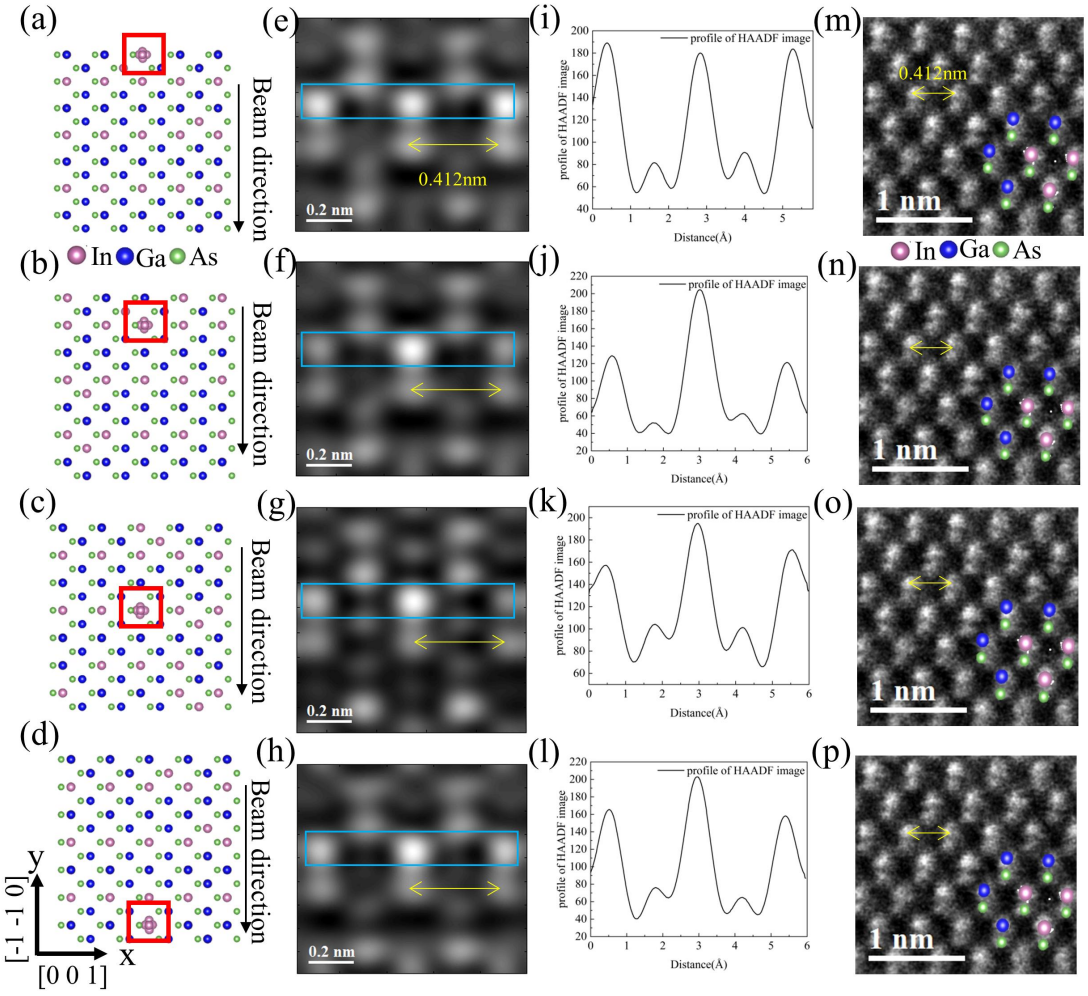

Figure 3: (a-d) Simulated STEM-HAADF images for In clusters at different depths, the zone axis was set as [110], (e-h) HAADF images simulated by QSTEM[28]; (i-l) line profiles of indicated sub-sections of simulated HAADF images; (m-p) experimental HAADF images.

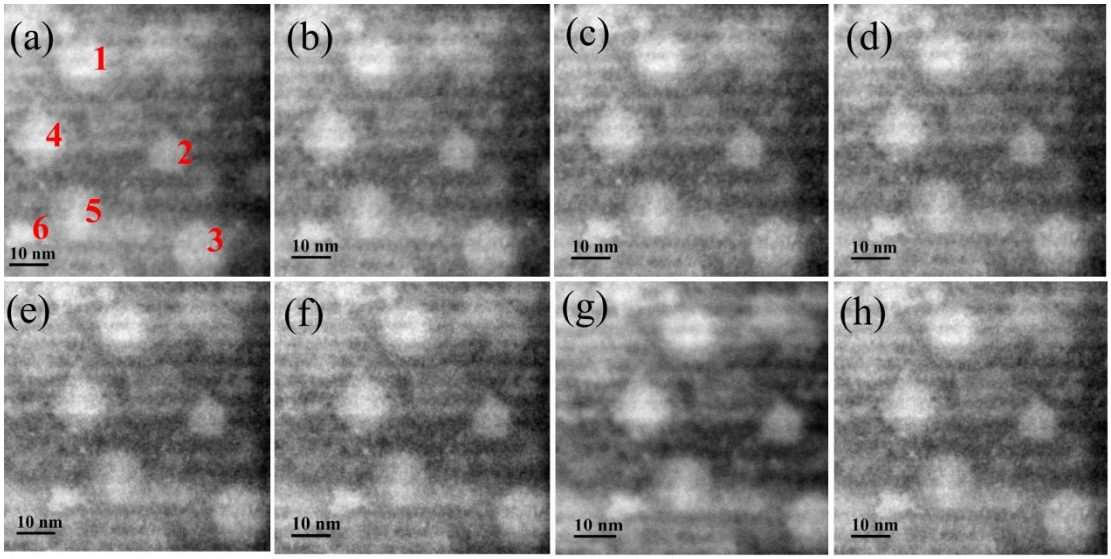

Figure 4: HAADF images of In clusters in quantum wells under different focus conditions at (a) -40 nm, (b) -30 nm, (c) -20 nm, (d) -9.7 nm, (e) 10 nm, (f) 20 nm, (g) 100 nm and (h) 243 nm. For the Focus Series imaging, we adopted a beam current of 170 pA, the dwell time was set as 10 µs with a scan speed of ~1×10^5 pixel per second, so the dose can be estimated as 2.23×10^{20} electrons/cm^2 during the image acquisition.

Defocus / Number	-40nm	-30nm	-20nm	-9.7nm	10nm	20nm	100nm	243nm
1	13.98nm	13.95nm	14.01nm	13.97nm	14.02nm	13.93nm	13.96nm	13.94nm
2	11.49nm	11.46nm	11.51nm	11.45nm	11.42nm	11.43nm	11.5 nm	11.46nm
3	16.41nm	16.42nm	16.41nm	16.44nm	16.40nm	16.45nm	16.42nm	16.43nm
4	17.01nm	17.03nm	17.05nm	17.02nm	17.00nm	17.02nm	17.02nm	17.04nm
5	14.86nm	14.83nm	14.82nm	14.85nm	14.83nm	14.82nm	14.84nm	14.82nm
6	7.81nm	7.76nm	7.74nm	7.82nm	7.77nm	7.79nm	7.78nm	7.75nm

Table 1: Statistics of diameters of six In clusters in Figure 4 (a)-(h).

QSTEM simulation is exploited to investigate the visibility of In clusters at different depths. The In cluster considered in the simulations has been set to 3 interstitial In atoms within an $In_{0.5}Ga_{0.5}As$ random alloy. At 300 kV accelerating voltage, the convergence angle and inner collection angle were set as 25 mrad and

170 mrad respectively, in agreement with the experimental set-up. The total sample thickness was modelled as ~50 nm, where the lattice can be probed. The viewing direction has been set as [110] zone axis, so the simulated (Figs 3 (e)-(h)) and experimental (Figs. 3 (m)-(p)) atomic images can be directly compared. As shown in Fig. 3 (e-h) and (m-p) by yellow arrows, the atomic distance between atoms in the same horizontal plane in simulated and experimental images is about 0.412 nm (≈ a/ $\sqrt{2}$), indicating consistency between experimental and simulated images. By inserting the In clusters at different depths (0 nm, 1 nm, 16 nm, 41 nm), simulated HAADF images as shown in Figs. 3 (e)-(h) are obtained. As can be seen in the line scans of Figs. 3 (i)-(l), the In interstitials at different depths have no influence on the intensity profile of HAADF images (Figs 3 (i)-(l)), indicating small In clusters of a few interstitial atoms formed in the sample may remain invisible in HAADF imaging. Therefore, in Fig. 2 (a), several In interstitials may have segregated within the quantum wells, but are not apparent in the HAADF images. To determine whether growth of In clusters in Fig. 2 is due to the swelling of sub-critical In interstitial clusters, focus series of STEM-HAADF images were recorded, where the centre may contain multiple In clusters at different depths. As shown in Fig. 4 (a)-(h) and Table 1, the morphology and size of In clusters are independent of focus conditions. Therefore, it can be concluded that once In clusters are formed in the lamella sample, neither the cluster depth in the sample nor the focus condition would influence the swelling of cluster size. The lateral expansion of In-rich regions in Fig. 2 can only be explained by the promotion of In segregation due to electron irradiation, finally leading to In precipitates.

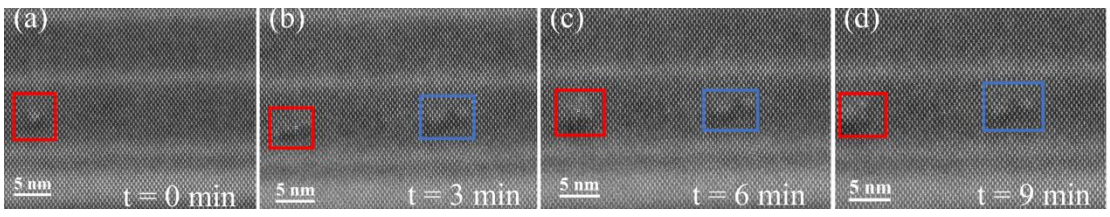

Figure 5: (a-d) Swelling of ln-rich clusters under continuous electron beam rastering.

As the QSTEM simulations in Fig. 3 show the problem in detecting tiny interstitial In clusters, such In clusters and certainly single In atoms displaced by Ga^+ implantation will initially be invisible in HAADF images but when such In clusters segregate under electron beam irradiation they may become visible during longer acquisition of HAADF images. The low plasmon energy of metallic In prevents a study of In segregation by VEELS at the atomic scale, due to the delocalization of inelastic scattering.[29] Extensive electron beam rastering was performed on a region where only 1 In cluster had originally been observed (at $t = 0$ min, red square in Fig. 5 (a)). After 3 minutes exposure to the electron beam, two additional In particles have emerged in the blue rectangular region in Fig. 5 (b), which were completely invisible in Fig. 5 (a). By further scanning the same region for 9 minutes, the morphology of In clusters in the blue region became significantly clearer. As no such clusters were observed in the Ar^+ ion thinned lamella, even after extended electron beam imaging, it can be concluded that small In clusters are triggered by Ga^+ ion beam irradiation and may be ignored in the early stage of HAADF imaging, however, during further electron irradiation, In segregation will continue and after some time form larger In precipitates that are metallic and will change the electronic properties of the material.

4 CONCLUSIONS

In summary, we have revealed the formation of In precipitates in InGaAs/InAlAs pre-formed under Ga^+ FIB sample preparation and subsequently expanded by electron beam irradiation. By comparing Ga^+ and Ar^+ ion milling techniques for electron beam transparent sample preparation, only the Ga^+ ions could give rise to the formation of small In clusters in InGaAs/InAlAs quantum wells. These tiny clusters are initially almost invisible in lattice images. In segregation is enhanced under subsequent electron irradiation, where the size of In-rich clusters formed is gradually increasing. Our finding provides the experimental evidence of Ga implantation induced In segregation and precipitation under electron irradiation. These findings emphasize the need for caution when studying FIB prepared InGaAs based III-V quantum well

specimens by transmission electron microscopy, even if initial In segregation appears invisible.

ACKNOWLEDGMENTS

This work was supported by the National Natural Science Foundation of China (grant number: 61975075), the Department of Science and Technology of Sichuan Province (grant number: 2023YFH0054), the Technology and Innovation Commission of the Shenzhen Municipality (grant number: JCYJ20190809142019365). The authors acknowledge the assistance of SUSTech Core Research Facilities and the help of Dr. Dong-Sheng He at Pico Center for the aberration corrected TEM experiments.

DATA AVAILABILITY

The data that support the findings of this study are available from the corresponding author upon reasonable request.

REFERENCES

1. Mayrock, O., Wünsche, H. J., & Henneberger, F. (2000) Polarization charge screening and indium surface segregation in (In, Ga)N/GaN single and multiple quantum wells. *Physical Review B*, 62, 92272-16880.
2. Lei, H., Chen, J., & Ruterana, P. (2010) Role of c-screw dislocations on indium segregation in InGaN and InAlN alloys. *Applied Physics Letters*, 96, 161901.
3. Waltereit, P., Brandt, O., Ploog, K. H., Tagliente, M. A., & Tapfer, L. (2001) Indium Surface Segregation during Growth of (In, Ga) N/GaN Multiple Quantum Wells by Plasma-Assisted Molecular Beam Epitaxy. *Physica Status Solidi (b)*, 228, 49-53.
4. Duxbury, N., Bangert, U., Dawson, P., Thrush, E. J., Van der Stricht, W., Jacobs, K., & Moerman, I. (2000) Indium segregation in InGaN quantum-well structures. *Applied Physics Letters*, 76, 1600-1602.

5. Mishra, P., Ramesh, V., Srinivasan, T., Singh, S. N., Goyal, A., Sharma, R. K., & Muralidharan, R. (2005) Observation of indium segregation effects in structural and optical properties of pseudomorphic HEMT structures. *Semiconductor Science and Technology*, 21, 131-137.
6. Choubani, M., Maaref, H., & Saidi, F. (2022) Indium segregation and In–Ga inter-diffusion effects on the photoluminescence measurements and nonlinear optical properties in lens-shaped $In_xGa_{1-x}As$/GaAs quantum dots. *Journal of Physics and Chemistry of Solids*, 160, 110360.
7. Klymenko, M. V., Sukhoivanov, I. A., & Shulika, O. V. (2012) Impact of indium surface segregation on optical properties of ultrathin InGaN/GaN quantum wells. *Gallium Nitride Materials and Devices VII*, 8262, 277-284.
8. Walther, T., Amari, H., Ross, I. M., Wang, T., & Cullis, A. G. (2013) Lattice resolved annular dark-field scanning transmission electron microscopy of (Al, In) GaN/GaN layers for measuring segregation with sub-monolayer precision. *Journal of Materials Science*, 48, 2883-2892.
9. MacArthur, K. E., Pennycook, T. J., Okunishi E., D'Alfonso, A. J., Lugg, N. R., Allen, L. J., & Nellist, P. D. (2013) Probe integrated scattering cross sections in the analysis of atomic resolution HAADF STEM images. *Ultramicroscopy*, 133, 109-119.
10. De Backer, A., Martinez, G. T., Rosenauer, A., & Van Aert, S. (2013) Atom counting in HAADF STEM using a statistical model-based approach: Methodology, possibilities, and inherent limitations. *Ultramicroscopy*, 134, 23-33.
11. Xia, D., Jiang, Y. B., Notte, J., & Runt, D. (2020) GaAs milling with neon focused ion beam: Comparison with gallium focused ion beam milling and subsurface damage analysis. *Applied Surface Science,* 538, 147922.
12. Tseng, A. A. (2005) Recent developments in nanofabrication using focused ion beams. *Small,* 1, 924-939.

13. Xia, D., Notte, J., Stern, L., & Goetze, B. (2015) Enhancement of XeF2-assisted gallium ion beam etching of silicon layer and endpoint detection from backside in circuit editing. *Journal of Vacuum Science & Technology B*, 33,2166-2746.
14. Giannuzzi, L. A., & Stevie, F. A. (1999) A review of focused ion beam milling techniques for TEM specimen preparation. *Micron*, 30, 197-204.
15. Spehner, D., Steyer, A. M., Bertinetti, L., Orlov, I., Benoit, L., Pernet-Gallay, K., Schertel A. & Schultz, P. (2020) Cryo-FIB-SEM as a promising tool for localizing proteins in 3D. *Journal of structural Biology*, 211, 107528.
16. M.W. Phaneuf. (1999) Applications of focused ion beam microscopy to materials science specimens. *Micron*, 30, 277-288.
17. Ma, Z., Zhang, X., Liu, P., Deng, Y., Hu, W., Chen, L., Zhu J., Chen S., Wang Z., Shi Y., Ma J., Wang X., Qiu Y., Zhang K., & Walther, T. (2023) Clustering in gallium ion beam sputtered compound materials driven by bond strength and interstitial/vacancy reaction. *Applied Physics Letters*, 123, 102101.
18. Dhara, S., Datta, A., Wu, C. T., Chen, K. H., Wang, Y. L., Muto, S., Tanabe T., Shen C. H., Hsu C. W., Chen L. C. & Maruyama, T. (2005) Mechanism of nanoblister formation in Ga^+ self-ion implanted GaN nanowires. *Applied Physics Letters*, 86, 386-396.
19. Zhang, S., Wang, B. W., Zhang, L. M., Liu, N., Wang, T. S., Duan, B. H., & Xu, X. G. (2021) Defect agglomeration induces a reduction in radiation damage resistance of In-rich $In_xGa_{1-x}N$. *Journal of Physics D: Applied Physics*, 54, 245104.
20. Yu, L., Hu, J., Ma, Y., & Zhao, L. (2023) Electron beam irradiation effects on GaN/InGaN multiple quantum well structures. *Semiconductor Science and Technology*, 38, 105001.
21. Nykänen, H., Mattila, P., Suihkonen, S., Riikonen, J., Quillet, E., Homeyer, E., Bellessa J. & Sopanen, M. (2011) Low energy electron beam induced damage on InGaN/GaN quantum well structure. *Journal of Applied Physics*, 109, 78.
22. Baloch, K. H., Johnston-Peck, A. C., Kisslinger, K., Stach, E. A., & Gradečak, S. (2013) Revisiting the "In-clustering" question in InGaN through the use of

aberration-corrected electron microscopy below the knock-on threshold. *Applied Physics Letters,* 102,191910.

23. O'Neill, J. P., Ross, I. M., Cullis, A. G., Wang, T., & Parbrook, P. J. (2003) Electron-beam-induced segregation in InGaN/GaN multiple-quantum wells. *Applied Physics Letters*, 83, 1965-1967.
24. Smeeton, T. M., Kappers, M. J., Barnard, J. S., Vickers, M. E., & Humphreys, C. J. (2003) Electron-beam-induced strain within InGaN quantum wells: False indium "cluster" detection in the transmission electron microscope. *Applied Physics Letters*, 83, 5419-5421.
25. Yang, C. C., Feng, S. W., Lin, Y. S., Cheng, Y. C., Liao, C. C., Tsai, C. Y., Ma K. J. & Chyi, J. I. (2001) Indium segregation in InGaN/GaN quantum well structures. *Ultrafast Phenomena in Semiconductors V*, 4280, 20-26.
26. Okuno, H., Takeguchi, M., Mitsuishi, K., Irokawa, Y., Sakuma, Y., & Furuya, K. (2010) Local characterizations of quaternary AlInGaN/GaN heterostructures using TEM and HAADF-STEM. *Surface and Interface Analysis*, 40, 1660-1663.
27. Bouslama, M., Ghamnia, M., Gruzza, B., Miloua, F., & Jardin, C. (1994) AES and EELS analysis of the interaction between phosphorus and metallic indium. *Journal of Electron Spectroscopy and related Phenomena*, 68, 377-382.
28. Woo, J., & Guliants, V. V. (2016) QSTEM-based HAADF-STEM image analysis of Mo/V distribution in MoVTeTaO M1 phase and their correlations with surface reactivity. *Applied Catalysis A: General*, 512, 27-35.
29. Egerton, R. F., Hayashida, M., & Malac, M. (2023) Transmission electron microscopy of thick polymer and biological specimens. *Micron*, 169, 103449.